

Article

# A Simple Colorimetric and Fluorescent Sensor to Detect Organophosphate Pesticides Based on Adenosine Triphosphate-Modified Gold Nanoparticles

Xiaoxia Li, Haixin Cui \* and Zhanghua Zeng \* 

Institute of Environment and Sustainable Development in Agriculture, Chinese Academy of Agricultural Sciences, Beijing 100081, China; lixiaoxia1292@gmail.com

\* Correspondence: cuihaixin@caas.cn (H.C.); zengzhanghua@caas.cn (Z.Z.)

Received: 18 October 2018; Accepted: 4 December 2018; Published: 6 December 2018



**Abstract:** A simple and dual modal (colorimetric and fluorescent) sensor for organophosphate pesticides with high sensitivity and selectivity using adenosine triphosphate (ATP)- and rhodamine B-modified gold nanoparticles (RB-AuNPs), was successfully fabricated. This detection for ethoprophos afforded colorimetric and fluorescence imaging changes visualization. The quantitative determination was linearly proportional to the amounts of ethoprophos in the range of a micromolar scale (4.0–15.0  $\mu\text{M}$ ). The limit of detection for ethoprophos was as low as 37.0 nM at  $3\sigma/k$ . Moreover, the extent application of this simple assay was successfully demonstrated in tap water samples with high reliability and applicability, indicating remarkable application in real samples.

**Keywords:** organophosphate pesticides; gold nanoparticles; colorimetric and fluorescent sensor; ethoprophos detection; multimodal assay

## 1. Introduction

Pesticides have been widely used worldwide to protect crops from insects and increase the quantity and quality of agricultural products [1–3]. Pesticide use, however, can affect ecosystems, nontarget organisms, agricultural product safety, and human health [4]. Organophosphates (OPs) are a class of pesticides designed to affect the insect nervous system [5–10]. OPs irreversibly inactivate acetylcholinesterase, an enzyme that degrades the neurotransmitter acetylcholine at cholinergic synapses and that is essential to nerve function [11,12]. OP residues in agricultural products and water are a potential source of toxicity to bees, wildlife, and humans [13,14]. It is therefore imperative to develop highly sensitive and reliable methods to determine pesticide content in environmental samples.

Multiple methods to assay OPs have been developed, including gas chromatography-mass spectrometry, liquid chromatography, enzyme inhibition, enzyme-linked immunosorbent assay (ELISA), and electrochemical analysis [15–21]. Chromatography is typically used for assaying pesticides, and liquid or gas chromatography-mass spectrometry is the most common method. Whereas chromatography methods provide adequate selectivity and sensitivity, they require multistep sample pretreatment, detailed experimental conditions, and adept operators and sophisticated instruments. The enzyme inhibition method is a fast and simple low-cost technique, but its specificity is low. ELISA uses antibodies and color changes to identify a substance with good repeatability, sensitivity, and specificity, but the poor stability of enzymes or antibodies in practical performance and the low specificity limit its use. None of the conventional methods are suitable for on-site detection with sensitivity and specificity. Significant challenges remain in exploiting fast, specific, low-cost, and easy-to-manipulate OP assays.

Gold nanoparticles (AuNPs) possess unique optical properties related to their size, surrounding environment, and dispersion state [22,23]. AuNP-based colorimetric and fluorescent assays have been used for chemical and biological applications with versatility and simplicity [24–30]. These assays are based on AuNP dispersion and aggregation states in response to a specific analyte and certain recognition mechanisms. The surface energy of AuNPs tends to decrease, leading to aggregation and sedimentation of the colloidal system. Citric acid-modified AuNPs can be easily aggregated by the addition of sulfur-containing OPs because of the strong Au-S bond. In recent years, this AuNP aggregation mechanism has drawn considerable attention in OP research [31–34]. Although these methods are accurate, fast, sensitive, and easy to perform, they commonly lack specificity to some OPs because of the sensitive, strong Au-S bond, as many OPs contain sulfur. In theory, electrostatic and steric repulsion are the two main stabilizing mechanisms against AuNP aggregation, and the strong Au-S bond can destroy AuNP electrostatic stabilization and result in aggregation, depending on the OPs' sulfur energy and capping agents. In this paper, we discuss the possibility of identifying and quantifying specific sulfur-containing OPs by controlling the Au-S bond and capping agent. We established a specific dual-readout assay for the OP ethoprophos by adding adenosine triphosphate (ATP) to AuNPs and controlling the ratio of ATP to AuNPs. This method was validated in tap water sample analysis.

## 2. Materials and Methods

### 2.1. Chemicals and Instruments

Chlorpyrifos (CP), ethoprophos (EP), profenofos (PF), trichlorfon (TC), omethoate (OT), monocrotophos (MC), isocarbophos (IC), and malathion (MT) were purchased from Honeywell Fluka (Morris Plains, NJ, USA). Adenosine 5'-triphosphate disodium salt hydrate (ATP) was obtained from Sigma-Aldrich (St. Louis, MO, USA). Gold(III) chloride trihydrate (49.0% Au) and sodium citrate tribasic dihydrate were purchased from J&K Scientific (Beijing, China). All commercial chemicals were used directly without any purification.

The color changes caused by AuNP aggregation were measured by ultraviolet-visible light spectroscopy absorption (400–900 nm) using a Shimadzu 2600 spectrophotometer (Shimadzu Corp., Kyoto, Japan). Because the AuNP solution was highly concentrated, we double-diluted the solution and set the corresponding absorption band to 520 nm. The fluorescence intensity of the spectra was recorded at a range of 540–700 nm, operating at an excitation wavelength of 520 nm using a Hitachi F7000 fluorescence spectrophotometer (Hitachi, Tokyo, Japan). The weak fluorescence intensity of rhodamine B-AuNP (RB-AuNP) solutions at approximately 565 nm indicated that the fluorescence of the rhodamine B molecules was completely quenched by the AuNPs, confirming that nearly all rhodamine B molecules were adsorbed onto the surfaces of the AuNPs. The excitation and emission slit widths were both 10 nm. Fluorescence intensities were captured using an inverted fluorescence microscope (Olympus, Tokyo, Japan). The diameter and morphology of AuNPs were imaged by transmission electron microscope (Hitachi HT7700), and hydrodynamic size distribution was measured using a particle size analyzer (Nano-ES90, Malvern Instruments, Malvern, UK).

### 2.2. Preparation of Stock Solutions

Stock solutions of the pesticides (10.0 mM) were prepared in absolute ethanol and used within one month. The pesticide stock solutions were diluted 10-fold with absolute ethanol, to obtain 1.0 mM solutions.

The standard serial solution of ethoprophos was one milliliter of 1.0 mM ethoprophos solution transferred to a 50-mL volumetric flask and diluted with deionized water to a specific volume, then fully mixed. The final concentration was 20.0  $\mu$ M. Aliquots (1.0, 2.0, 3.0, 4.0, 5.0, and 7.5 mL) of the pre-prepared ethoprophos (20.0  $\mu$ M) solution were transferred to 10.0-mL volumetric flasks, diluted with deionized water to a specific volume, and fully mixed. The corresponding concentrations of these serial solutions were 2.0, 4.0, 6.0, 8.0, 10.0, and 15.0  $\mu$ M.

ATP (10.0 mM) and rhodamine B (10.0 mM) were prepared in deionized water and used within one week. For lower concentrations of solutions used in later experiments, the ATP and rhodamine B stock solutions were diluted with deionized water and used within 8 h.

### 2.3. Preparation of AuNPs

The AuNPs used in this experiment were water-soluble and had diameters of approximately 13 nm, as determined by transmission electron microscopy. The sodium citrate solution preparation described by Hauser and Lynn was used to synthesize citrate-capped hydrophilic AuNPs [35]. By varying the citrate/Au<sup>3+</sup> molar ratio according to the modification by Turkevich and Frens [36], the diameters of the AuNPs were tuned to a range of 10–150 nm.

### 2.4. Citrate-Capped Hydrophilic AuNPs

HAuCl<sub>4</sub> (40.2 mg, 49.0% Au) was dissolved in 100.0 mL deionized water and heated to boiling. The HAuCl<sub>4</sub> solution appeared yellow. Ten milliliters of trisodium citrate solution (38.8 mmol/L) were then added slowly to the HAuCl<sub>4</sub> solution with stirring. Color changes accompanied the reaction, from yellow to dark blue to a final transparent wine-red. The solution was heated for another 10.0 min. After cooling to room temperature, the obtained aqueous citrate-capped AuNP solution was filtered through a 0.22- $\mu$ m hydrophilic membrane to remove insoluble residues and large solid particles.

### 2.5. Preparation of ATP-Modified AuNPs and Rhodamine B-Coated AuNPs

AuNPs were protected by ATP before coating with rhodamine B. First, a stock solution of ATP (1.0 mM, 1.0 mL) was added to the citrate-capped hydrophilic AuNPs solutions (50.0 mL). The mixed solutions were vortexed for 30.0 min at room temperature. Next, 1.5 mL rhodamine B solutions (1.0  $\mu$ M) were slowly added to the ATP-protected AuNPs solutions and vortexed lightly in the dark at room temperature for 30.0 min. The resulting RB-AuNPs solutions were stored at 4.0 °C as stock solutions for later use. The particle size of the RB-AuNPs was approximately 15 nm, and the particles were mono-dispersed in the solution.

### 2.6. Citrate-Capped AuNPs Pesticide Assay

Citrate-capped AuNPs were first double-diluted for this experiment. The pesticide solutions (50.0  $\mu$ L, 1.0 mM) were added to the double-diluted citrate-capped AuNPs solutions (5.0 mL). Ethanol (50.0  $\mu$ L) was added to the citrate-capped AuNPs solution (5.0 mL) as a blank, which eliminated interference and improved the precision of analysis. The blank test was repeated for 12 replicates to calculate the limit of detection (LOD). The mixtures were vortexed for 1.0 min and kept in the dark for 15.0 min before being imaged, and the ultraviolet-visible light absorption spectra (400–900 nm) were collected. All measurements were repeated for at least three replicates.

### 2.7. ATP-Protected AuNPs Pesticide Assay

The experimental procedure and conditions for the citrate-capped AuNPs assay were repeated, replacing citrate-capped AuNPs with RB-AuNPs. The solutions were imaged and the ultraviolet-visible light absorption spectra (400–900 nm) were collected. All measurements were repeated for at least three replicates.

### 2.8. Experimental Procedure for Ethoprophos Detection Sensitivity

The standard ethoprophos serial solutions (0.5–100.0  $\mu$ M) were mixed with the RB-AuNPs in a ratio of 1:1 in ultramicro cells (Agilent Technologies, Santa Clara, CA, USA), vortexed for 20 s, and the ultraviolet-visible light absorption spectra (400–900 nm) were recorded every 1 min 30 times. The LOD was calculated as  $3\sigma/k$ , where  $\sigma$  is the standard deviation of the 12 blank tests, and  $k$  is the slope of the linear fitting equation.

### 3. Results and Discussion

#### 3.1. Aggregation-Inducing Effect of OPs on Citrate-Capped AuNPs

We first analyzed the aggregation-inducing effect of the OPs (Figure 1) on citrate-capped AuNPs (Figure 2a). We calculated the absorption change at 520 nm ( $\Delta A_{520}$ ) by setting the blank value as zero. The corresponding LOD was also adjusted by deducting the blank value. We found that ethoprophos, profenofos, and chlorpyrifos induced aggregation of citrate-capped AuNPs. This was confirmed by the AuNPs' color changes from red to purple and blue. The  $\Delta A_{520}$  was 0.809 (ethoprophos, 10.0  $\mu\text{M}$ ), 0.399 (profenofos, 10.0  $\mu\text{M}$ ), and 0.129 (chlorpyrifos, 10.0  $\mu\text{M}$ ). The AuNP solutions did not change color in the presence of the other pesticides (1.0 mM) or ethanol. The  $\Delta A_{520}$  for malathion could not be determined. The  $\Delta A_{520}$  values of trichlorfon, omethoate, monocrotophos, isocarbofos, and malathion were determined to be much smaller than those of ethoprophos and profenofos (Figure 2). These findings indicated that although a visible aggregation of citrate-capped AuNPs was not observed, these four pesticides could cause a slight aggregation of citrate-capped AuNPs.

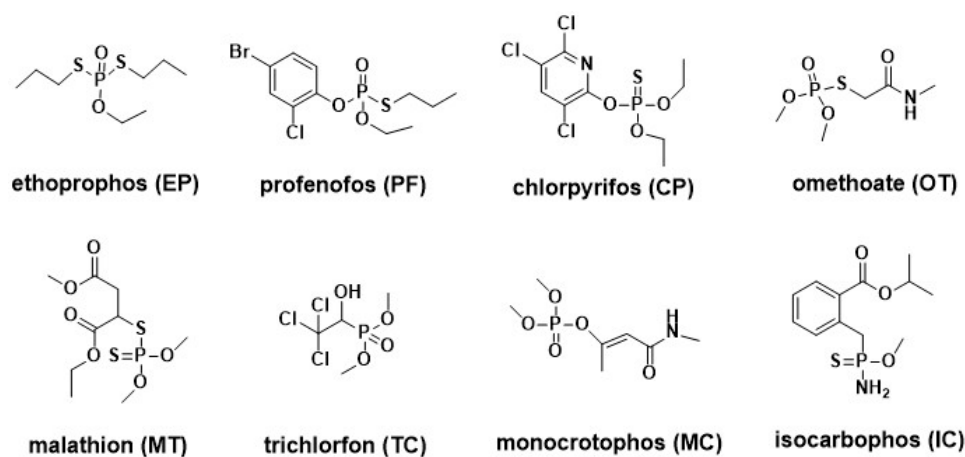


Figure 1. The structure of organophosphate (OP) pesticides.

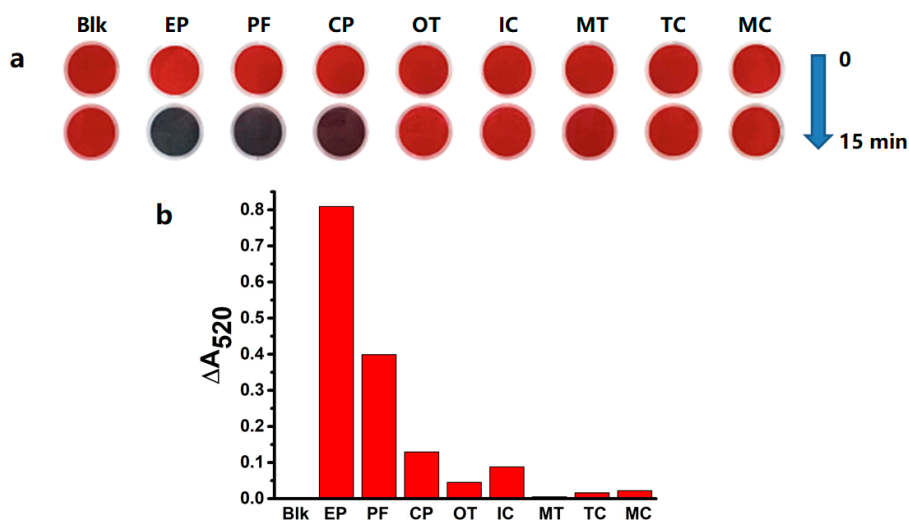


Figure 2. (a) The color changes of citrate-capped gold nanoparticles (AuNPs) (3.0 nM) added with various pesticides (10.0  $\mu\text{M}$  for ethoprophos, profenofos, and chlorpyrifos; 1.0 mM for others). (b) The  $\Delta A_{520}$  values changes of citrate-capped AuNPs (3.0 nM) added with various OPs pesticides (10.0  $\mu\text{M}$  for ethoprophos, profenofos, and chlorpyrifos; 1.0 mM for others).

### 3.2. Colorimetric and Fluorescent Detection of OPs by RB-AuNPs

To improve the detection specificity of AuNPs for OPs, we measured the effects of OPs on RB-AuNPs, which were capped with ATP on the surface. ATP has a greater affinity for AuNPs than citric acid, because both adenine and triphosphate show some binding to AuNPs. This binding affinity is ATP concentration-dependent. We envisioned that AuNPs capped with a specific concentration could show specific assays for OPs based on the displacement of ATP and OPs. To selectively assay for ethoprophos, an ATP concentration was optimized to be 1.2 mM (a detailed discussion is presented in the next section). As expected, only ethoprophos caused a color change in RB-AuNPs, from wine-red to a pink color within 15.0 min (Figure 3a), indicating improved specificity for ethoprophos compared to findings from citrate-capped AuNPs (Figure 3b). The absorption responses of RB-AuNPs to ethoprophos were concentration-dependent (Figure 3c). Ethoprophos yielded a relatively large positive  $\Delta A_{520}$  of 0.205, and the color of the RB-AuNPs changed: The change was correlated with the concentration of ethoprophos (Figure 3c). The absorption at 520 nm decreased along with an increase at 600 nm, and the curve of the ratio of absorption at 600 nm and 520 nm ( $ROA_{600/520}$ ) versus ethoprophos concentration was plotted (Figure 3d). These results were indicative of RB-AuNPs' aggregation, which was confirmed by transmission electron microscopy (Figure 4). Profenofos (10.0  $\mu\text{M}$ ) had a rather low  $\Delta A_{520}$  of 0.028, without a color change. The  $\Delta A_{520}$  values of the other six OPs pesticides (1.0 mM) were very small, and the color of the AuNPs did not change. In addition, the competition experiments were studied by measuring  $ROA_{600/520}$  in the presence of ethoprophos (4.0  $\mu\text{M}$ ) and interfering analytes with a specific concentration (4.0  $\mu\text{M}$ ). Very few changes in  $ROA_{600/520}$  were observed in the combination of ethoprophos and interfering pesticides, indicating that this simple assay for ethoprophos could be applicable in the complex samples.

It is well known that AuNPs quench fluorophore fluorescence almost completely. Here, rhodamine B molecules were tightly adsorbed to the surface of AuNPs via electrostatic attraction to ATP, which was confirmed by the negligible fluorescence intensity of the RB-AuNPs. The fluorescent results showed that RB-AuNPs had a strong, concentration-dependent fluorescence recovery response to ethoprophos (Figure 5) and a negligible response to the other OPs.

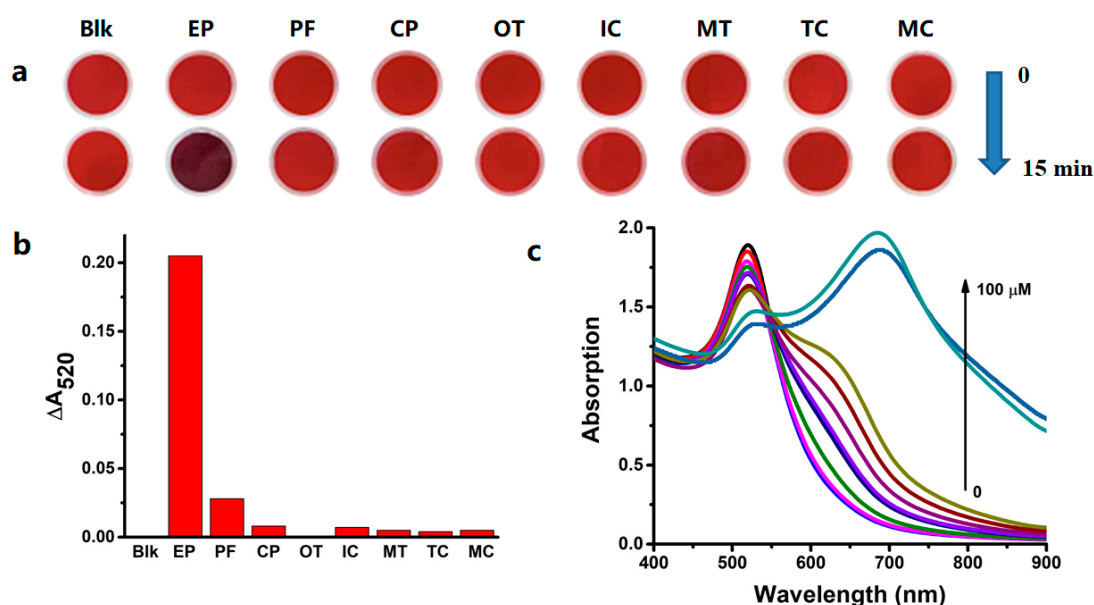
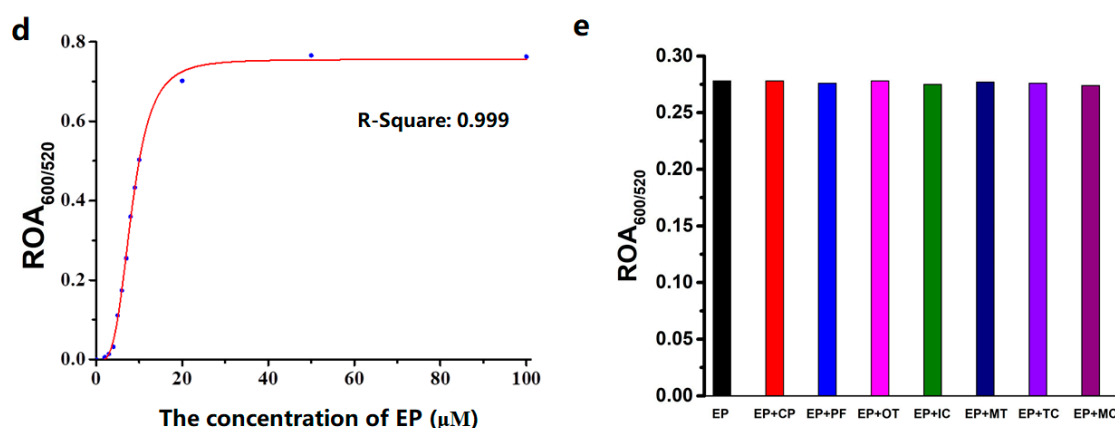
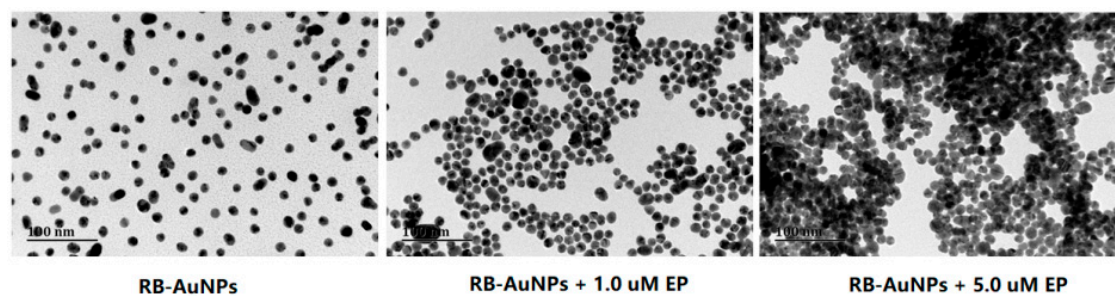


Figure 3. Cont.



**Figure 3.** (a) The color changes of rhodamine B (RB)-AuNPs (3.0 nM) added with various pesticides (10.0 μM for ethoprophos, profenofos, and chlorpyrifos; 1.0 mM for others). (b) The  $\Delta A_{520}$  values changes of RB-AuNPs (3.0 nM) added with various OP pesticides (10.0 μM for ethoprophos, profenofos, and chlorpyrifos; 1.0 mM for others). (c) The absorption spectra changes and (d) corresponding fitting curve plot of RB-AuNPs (3.0 nM) in the presence of different concentrations of ethoprophos. (e) Selectivity studies of RB-AuNPs by measuring ROA<sub>600/520</sub> versus interference analytes with a specific concentration.



**Figure 4.** TEM images of RB-AuNPs (3.0 nM) added with various amount of ethoprophos. The scale bar is 100.0 nm.

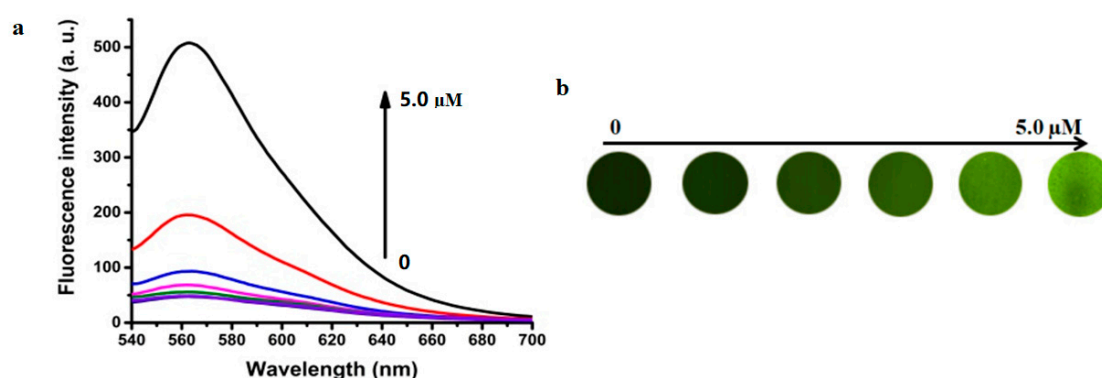


**Figure 5.** (a) The variation of fluorescence intensity and (b) fluorescence imaging of RB-AuNPs (3.0 nM) added with various amounts of ethoprophos (EP) (0–5.0 μM).

### 3.3. The Effect of ATP Concentration on OP Detection by RB-AuNPs

We found that after modification of the AuNPs with ATP, OP-induced aggregation of the NPs was inhibited to some extent. In the first experiment, using citrate-capped AuNPs, the OPs ethoprophos, profenofos, and chlorpyrifos caused notable aggregation of AuNPs, visualized by the color change from wine-red to dark blue after 15 min. Added ATP, however, replaced citric acid as the stabilizing agent,

as ATP has a greater affinity to AuNPs [37–39]. RB-AuNPs were not induced to aggregate by profenofos or chlorpyrifos, but only by ethoprophos. The corresponding  $\Delta A_{520}$  change in ultraviolet-visible light absorption declined markedly from 0.809 to 0.205, indicating that ATP enhanced AuNPs' stability and reduced the tendency to aggregate. Citrate-capped AuNPs had slight absorption responses to the other pesticides, whereas RB-AuNPs were not responsive. These findings suggest that ATP is protective of AuNPs and reduces OP-induced aggregation.

ATP concentrations and the detection reaction time were determining factors in this assay. Changes in the absorption spectra and color of RB-AuNPs were negligible for chlorpyrifos, trichlorfon, omethoate, monocrotophos, isocarbophos, and malathion, even at a high concentration of 50.0 mM. In the case of profenofos, slight variations in the absorption spectra and color of the RB-AuNPs were observed at low ATP concentrations or short reaction times of detection, suggesting that it may interfere with detecting ethoprophos. By optimizing the amount of ATP, we further tested various concentration of ATP. The results showed that the response to ethoprophos was in the range of 0.8–1.4 mM. At low concentrations of ATP, the sensitivity of the assay for ethoprophos was high. However, the RB-AuNPs showed some response to profenofos. At high concentrations of ATP, the sensitivity of the assay for ethoprophos was low, as there was no response to profenofos. As a result, the RB-AuNPs showed some response to profenofos in the low concentrations, and it took a long time to assay ethoprophos in the high concentrations. Given specificity and quickness, 1.0–1.2 mM ATP was optimized as a final concentration range. This established a method for detecting ethoprophos exclusively. The detailed data are summarized in Table 1. For the reported AuNPs-based OP sensors (Table 2), most of them were based on the inactivation of acetylcholinesterase and presented a lack of selectivity. Compared with them, this assay exhibited much more specificity and simplicity in the detection of ethoprophos.

**Table 1.** The  $\Delta A_{520}$  of RB-AuNPs with ethoprophos (10.0  $\mu\text{M}$ ) and profenofos (10.0  $\mu\text{M}$ ) in the various concentrations of adenosine triphosphate (ATP).

Pesticides	$\Delta A_{520}$	5 min	10 min	15 min	20 min	25 min	30 min
Ethoprophos	0.8 mM ATP	0.154	0.257	0.366	0.427	0.459	0.499
	1.0 mM ATP	0.051	0.107	0.205	0.289	0.366	0.472
	1.2 mM ATP	0.026	0.077	0.140	0.196	0.244	0.304
	1.4 mM ATP	0.012	0.058	0.119	0.172	0.220	0.284
Profenofos	0.8 mM ATP	ND	0.025	0.039	0.048	0.056	0.061
	1.0 mM ATP	ND	0.018	0.021	0.035	0.042	0.049
	1.2 mM ATP	ND	ND	ND	0.015	0.023	0.030
	1.4 mM ATP	ND	ND	ND	ND	ND	ND

ND means not detected.

**Table 2.** The reported AuNP-based OP sensors.

Target Analyte	Detection Technique	Linear Range	Detection Limit	References
OPs	Colorimetric/fluorescence	ND	ND	[31]
OPs	Fluorescence	ND	0.05 ng/mL	[40]
OPs	Electrochemistry	0.001–5 $\mu\text{M}$	0.5 nM	[41]
OPs	Colorimetric	ND	2 ppm	[42]
Chlorpyrifos/malathion	Colorimetric	100–250 ppb	20 ppb	[43]
OPs	Colorimetric	80–400 ng/mL	30 ng/mL	[32]
OPs	Colorimetric	15–65 ppb	0.7 ppb	[34]
Paraoxon	Electrochemistry	ND	0.1 pM	[44]
Monocrotophos	Electrochemistry	ND	2.7 nM	[45]
Ethoprophos	Colorimetric/fluorescence	4–15 $\mu\text{M}$	37 nM	This work

ND means not detected.

### 3.4. The pH Effect on the Colorimetric Assay for Ethoprophos

Usually, pH shows a great effect on AuNP-based colorimetric sensors. The pH effect on this assay was studied in detail. Figure 6 reveals the  $\Delta A_{520}$  of RB-AuNPs with 10.0  $\mu\text{M}$  ethoprophos at various pH values (from 3.0 to 10.0). The  $\Delta A_{520}$  of RB-AuNPs in the presence of ethoprophos was stable (around 0.8) under acidic and weakly basic conditions. However, it dramatically changed to 0.04 at pH 10.0, probably due to the decomposition of ethoprophos under basic conditions. These results suggest that this assay is practical and applicable under broad pH conditions.

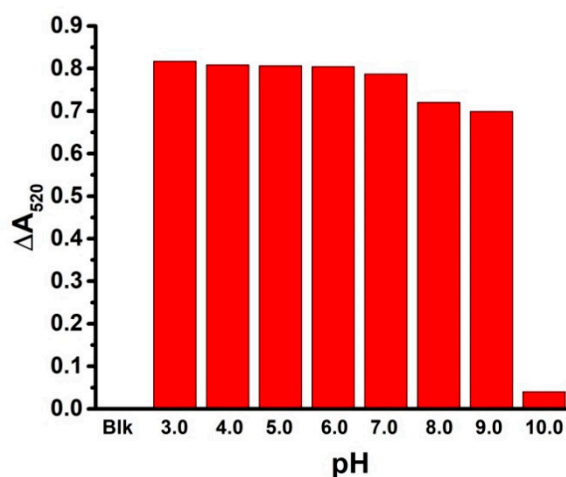
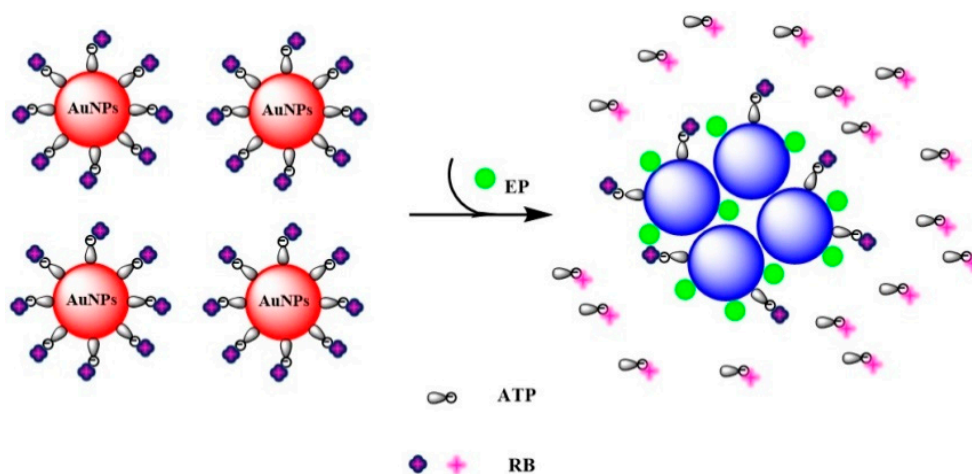


**Figure 6.** The pH effect on the assay for ethoprophos (10.0  $\mu\text{M}$ ) based on the measurement of  $\Delta A_{520}$  of RB-AuNPs.

### 3.5. Mechanism for Ethoprophos Detection

Sulfur-containing OPs can replace citric acid and lead to aggregation of AuNPs because of a strong Au-S binding tendency. ATP has high affinity for AuNPs, and can be considered a good stabilizing agent: ATP molecules adsorbed to the surface of RB-AuNPs can compete with sulfur-containing OPs, depending on the ATP concentration. Therefore, a specific assay for detecting sulfur-containing OPs could be refined by ATP concentration. Ethoprophos has a great affinity for AuNPs because it contains two sulfur atoms and forms stronger Au-S bonds than other OPs. It can demolish the frameworks of RB-AuNPs to cause nanoparticles aggregation, affording colorimetric change and fluorescence recovery (Scheme 1). An assay for ethoprophos could therefore be established if the ATP concentration was appropriate.



**Scheme 1.** The proposed mechanism of colorimetric and fluorescence detection for ethoprophos using RB-AuNPs.

### 3.6. Ethoprophos LOD in RB-AuNPs

We used various concentrations of ethoprophos (0–20.0  $\mu\text{M}$ ) to study the absorption spectra of RB-AuNPs, and found that the decrease of adsorption at 520 nm and the increase of adsorption at 600 nm correlated with ethoprophos concentration (Figure 7b). The variations in absorption spectra indicated the extent of RB-AuNPs' aggregation. The colorimetric variation was observed in this range (Figure 7a). The ratio of the absorption value at 600 nm to the absorption value at 520 nm at various ethoprophos concentrations was plotted to calculate the LOD, which was determined to be 0.089 mg/L (37.0 nM) at  $3\sigma/k$ . The quantitative range was 4.0–15.0  $\mu\text{M}$ .

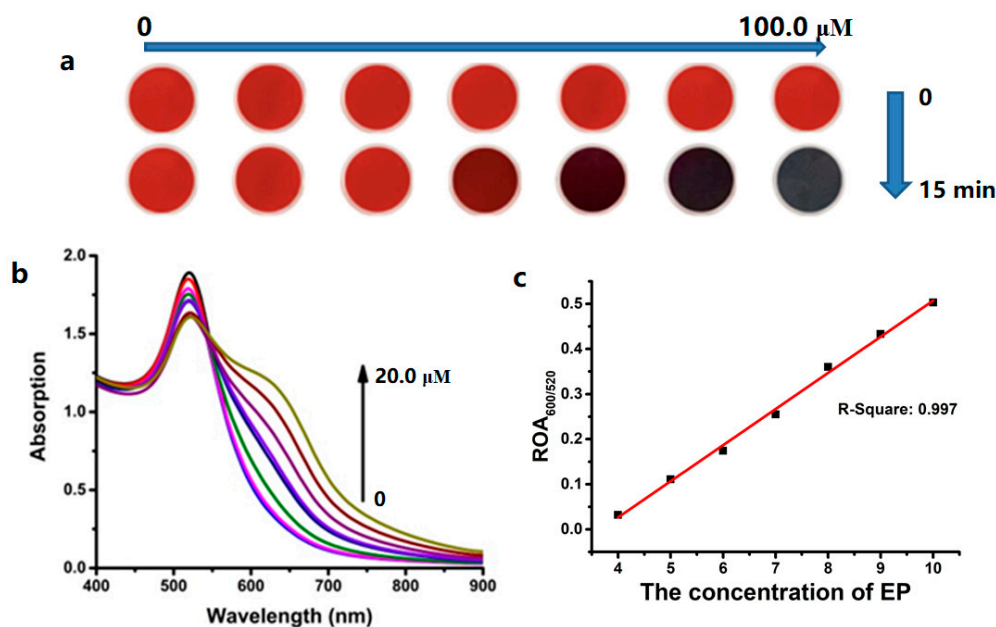


**Figure 7.** (a) The colorimetric and (b) absorption changes of RB-AuNPs in various amounts of ethoprophos. (c) The linear fitting of ROA<sub>600/520</sub> based on RB-AuNPs in the range of 4.0–10.0  $\mu\text{M}$  ethoprophos.

### 3.7. Ethoprophos Detection in Real Samples

Ethoprophos is commonly used for nematode control, and off-target spraying pollutes the surrounding environment and sources of drinking water. We used our RB-AuNPs assay to detect ethoprophos in tap water, anticipating that the complex matrices in a real sample would not interfere with accurate detection. A certain amount of ethoprophos was sprayed into tap water, and the obtained solution was concentrated to a specific volume and applied to RB-AuNPs. Table 3 shows that the ethoprophos recoveries were 102.4%, 105.4%, and 1.3.6%, based on the ratio of the absorption value at 600 nm to the absorption value at 520 nm. These findings confirmed that this method is applicable for detecting ethoprophos in real samples.

**Table 3.** The determination of ethoprophos in tap water samples based on this assay.

Samples	Spike ( $\mu\text{M}$ )	Found ( $\mu\text{M}$ )	Recovery (%)	RSD ( $n = 5$ ) <sup>a</sup>
1	4.0	4.1	102.6%	3.45%
2	8.0	8.4	105.4%	0.60%
3	10.0	10.4	103.6%	0.24%

<sup>a</sup> RSD = relative standard deviation.

#### 4. Conclusions

In this study, a simple colorimetric and fluorometric assay for detecting ethoprophos with high sensitivity and specificity using RB-AuNPs was established. The assay relied on ligand replacement on the surface of AuNPs, resulting in AuNP aggregation. This aggregation, in turn, permitted colorimetric visualization and fluorescence enhancement. The linear range of detection was calculated at the submicromolar level, and the LOD was determined to be 37.0 nM. This simple method was successfully applied to detect ethoprophos in tap water with high reliability. It is believed that this simple assay can be useful in monitoring ethoprophos on-site, especially in combination with other methods such as lab-on-chip techniques.

**Author Contributions:** Z.Z. and H.C. designed the experiments; X.L. carried out the experiments and analyzed the experimental results. Z.Z., H.C. and X.L. wrote the manuscript.

**Funding:** This work was funded by the National Key R&D Program of China (2017YFD0200900), Chinese Academy of Agricultural Sciences and National Key Basic Research Program of China (973 Program, 2014CB932200).

**Conflicts of Interest:** The authors declare no conflict of interest.

#### References

1. Mogul, M.G.; Akin, H.; Hasirci, N.; Trantolo, D.J.; Gresser, J.D.; Wise, D.L. Controlled Release of Biologically Active Agents for Purposes of Agricultural Crop Management. *Resour. Conserv. Recycl.* **1996**, *16*, 289–320. [[CrossRef](#)]
2. *International Code of Conduct on the Distribution and Use of Pesticides*; Food and Agriculture Organization of the United Nations: Rome, Italy, 2007.
3. Lamberth, C.; Jeanmart, S.; Luksch, T.; Plant, A. Current Challenges and Trends in the Discovery of Agrochemicals. *Science* **2013**, *341*, 742–746. [[CrossRef](#)] [[PubMed](#)]
4. Grube, A.; Donaldson, D.; Kiely, T.; Wu, L. *Pesticides Industry Sales and Usage*; U.S. Environmental Protection Agency: Washington, DC, USA, 2011.
5. Jamal, G.A. Neurological syndromes of organophosphorus compounds. *Toxicol. Rev.* **1997**, *16*, 133–170.
6. Roast, S.D.; Thompson, R.S.; Donkin, P.; Widdows, J.; Jones, M.B. Toxicity of the organophosphate pesticides chlorpyrifos and dimethoate to *Neomysis integer* (Crustacea: Mysidacea). *Water Res.* **1999**, *33*, 319–326. [[CrossRef](#)]
7. Dawson, A.H.; Eddleston, M.; Senarathna, L.; Mohamed, F.; Gawarammana, I.; Bowe, S.J.; Manuweera, G.; Buckley, N.A. Acute Human Lethal Toxicity of Agricultural Pesticides: A Prospective Cohort Study. *PLoS Med.* **2010**, *7*, e1000357. [[CrossRef](#)] [[PubMed](#)]
8. Battaglin, W.; Fairchild, J. Potential toxicity of pesticides measured in midwestern streams to aquatic organisms. *Water Sci. Technol.* **2002**, *45*, 95–102. [[CrossRef](#)] [[PubMed](#)]
9. Kim, K.; Tsay, O.G.; Atwood, D.A.; Churchill, D.G. Destruction and Detection of Chemical Warfare Agents. *Chem. Rev.* **2011**, *111*, 5345–5403. [[CrossRef](#)]
10. Aragay, G.; Pino, F.; Merkoci, A. Nanomaterials for Sensing and Destroying Pesticides. *Chem. Rev.* **2012**, *112*, 5317–5338. [[CrossRef](#)]
11. Mileson, B.E.; Chambers, J.E.; Chen, W.L.; Dettbarn, W.; Ehrich, M.; Eldefrawi, A.T.; Gaylor, D.W.; Hamernik, K.; Hodgson, E.; Karczmar, A.G.; et al. Common mechanism of toxicity: A case study of organophosphorus pesticides. *Toxicol. Sci.* **1998**, *41*, 8–20.
12. Ray, D.E. Chronic effects of low level exposure to anticholinesterases—A mechanistic review. *Toxicol. Lett.* **1998**, *102*, 527–533. [[CrossRef](#)]
13. Eyer, P. The Role of Oximes in the Management of Organophosphorus Pesticide Poisoning. *Toxicol. Rev.* **2003**, *22*, 165–190. [[CrossRef](#)] [[PubMed](#)]
14. Eddleston, M.; Buckley, N.A.; Eyer, P.; Dawson, A.H. Management of acute organophosphorus pesticide poisoning. *Lancet* **2008**, *371*, 597–607. [[CrossRef](#)]
15. Lambropoulou, D.A.; Albanis, T.A. Methods of sample preparation for determination of pesticide residues in food matrices by chromatography–mass spectrometry-based techniques: A review. *Anal. Bioanal. Chem.* **2007**, *389*, 1663–1683. [[CrossRef](#)] [[PubMed](#)]

16. Zhou, T.; Xiao, X.H.; Li, G.K. Microwave Accelerated Selective Soxhlet Extraction for the Determination of Organophosphorus and Carbamate Pesticides in Ginseng with Gas Chromatography/Mass Spectrometry. *Anal. Chem.* **2012**, *84*, 5816–5822. [[CrossRef](#)] [[PubMed](#)]
17. Qian, G.L.; Wang, L.M.; Wu, Y.R.; Zhang, Q.; Sun, Q.; Liu, Y.; Liu, F.Q. A monoclonal antibody-based sensitive enzyme-linked immunosorbent assay (ELISA) for the analysis of the organophosphorous pesticides chlorpyrifos-methyl in real samples. *Food Chem.* **2009**, *117*, 364–370. [[CrossRef](#)]
18. Viswanathan, S.; Radecka, H.; Radecki, J. Electrochemical biosensor for pesticides based on acetylcholinesterase immobilized on polyaniline deposited on vertically assembled carbon nanotubes wrapped with ssDNA. *Biosens. Bioelectron.* **2009**, *24*, 2772–2777. [[CrossRef](#)] [[PubMed](#)]
19. Yong, D.M.; Liu, C.; Yu, D.B.; Dong, S.J. A sensitive, rapid and inexpensive way to assay pesticide toxicity based on electrochemical biosensor. *Talanta* **2011**, *84*, 7–12. [[CrossRef](#)] [[PubMed](#)]
20. Xie, C.G.; Li, H.F.; Li, S.Q.; Wu, J.; Zhang, Z.P. Surface Molecular Self-Assembly for Organophosphate Pesticide Imprinting in Electropolymerized Poly(p-aminothiophenol) Membranes on a Gold Nanoparticle Modified Glassy Carbon Electrode. *Anal. Chem.* **2010**, *82*, 241–249. [[CrossRef](#)]
21. Periasamy, A.P.; Umasankar, Y.; Chen, S.M. Nanomaterials—Acetylcholinesterase Enzyme Matrices for Organophosphorus Pesticides Electrochemical Sensors: A Review. *Sensors* **2009**, *9*, 4034–4055. [[CrossRef](#)]
22. Klajn, R.; Stoddart, J.F.; Grzybowski, B.A. Nanoparticles functionalised with reversible molecular and supramolecular switches. *Chem. Soc. Rev.* **2010**, *39*, 2203–2237. [[CrossRef](#)]
23. Elghanian, R.; Storhoff, J.J.; Mucic, R.C.; Letsinger, R.L.; Mirkin, C.A. Selective Colorimetric Detection of Polynucleotides Based on the Distance-dependent Optical Properties of Gold Nanoparticles. *Science* **1997**, *277*, 1078–1081. [[CrossRef](#)] [[PubMed](#)]
24. Liu, J.; Lu, Y. A Colorimetric Lead Biosensor Using DNAzyme-Directed Assembly of Gold Nanoparticles. *J. Am. Chem. Soc.* **2003**, *125*, 6642–6643. [[CrossRef](#)] [[PubMed](#)]
25. Saha, K.; Agasti, S.S.; Kim, C.; Li, X.; Rotello, V.M. Gold Nanoparticles in Chemical and Biological Sensing. *Chem. Rev.* **2012**, *112*, 2739–2779. [[CrossRef](#)] [[PubMed](#)]
26. Guarise, C.; Pasquato, L.; De Fillippis, V.; Scrimin, P. Gold Nanoparticles-based Protease Assay. *Proc. Natl. Acad. Sci. USA* **2006**, *103*, 3978–3982. [[CrossRef](#)] [[PubMed](#)]
27. Liu, R.; Liew, R.; Zhou, J.; Xing, B. A Simple and Specific Assay for Real-Time Colorimetric Visualization of  $\beta$ -Lactamase Activity by Using Gold Nanoparticles. *Angew. Chem. Int. Ed.* **2007**, *46*, 8799–8803. [[CrossRef](#)] [[PubMed](#)]
28. Jiang, T.; Liu, R.; Huang, X.; Feng, H.; Teo, W.; Xing, B. A Gold-Nanoparticle Based Colorimetric Screening Method for Bacterial Enzymatic Inhibition. *Chem. Comm.* **2009**, *15*, 1972–1974. [[CrossRef](#)] [[PubMed](#)]
29. Nam, J.M.; Wise, A.R.; Groves, J.T. Colorimetric Bio-Barcode Amplification Assay for Cytokines. *Anal. Chem.* **2005**, *77*, 6985–6988. [[CrossRef](#)] [[PubMed](#)]
30. Zhou, W.; Gao, X.; Liu, D.; Chen, X. Gold Nanoparticles for In Vitro Diagnostics. *Chem. Rev.* **2015**, *115*, 10575–10636. [[CrossRef](#)]
31. Liu, D.; Chen, W.; Wei, J.; Li, X.; Wang, Z.; Jiang, X. A Highly Sensitive, Dual-Readout Assay Based on Gold Nanoparticles for Organophosphorus and Carbamate Pesticides. *Anal. Chem.* **2012**, *84*, 4185–4191. [[CrossRef](#)]
32. Fahimi-Kashani, N.; Hormozi-Nezhad, M.R. Gold-Nanoparticle-Based Colorimetric Sensor Array for Discrimination of Organophosphate Pesticides. *Anal. Chem.* **2016**, *88*, 8099–8106. [[CrossRef](#)]
33. Simoniana, A.L.; Goodb, T.A.; Wang, S.; Wild, J.R. Nanoparticle-based optical biosensors for the direct detection of organophosphate chemical warfare agents and pesticides. *Anal. Chim. Acta* **2005**, *534*, 69–77. [[CrossRef](#)]
34. Wu, S.; Li, D.; Wang, J.; Zhao, Y.; Dong, S.; Wang, X. Gold nanoparticles dissolution based colorimetric method for highly sensitive detection of organophosphate pesticides. *Sens. Actuator B Chem.* **2017**, *238*, 427–433. [[CrossRef](#)]
35. Turkevich, J.; Stevenson, P.C.; Hillier, J. A study of the nucleation and growth processes in the synthesis of colloidal gold. *Discuss. Faraday Soc.* **1951**, *11*, 55–75. [[CrossRef](#)]
36. Alfred, H.E.; Lynn, J.E. *Experiments in Colloid Chemistry*; McGraw-Hill book Company: New York, NY, USA, 1940.
37. Opdahl, A.; Petrovykh, D.Y.; Kimura-Suda, H.; Tarlov, M.J.; Whitman, L.J. Independent control of grafting density and conformation of single-stranded DNA brushes. *Proc. Natl. Acad. Sci. USA* **2007**, *104*, 9–14. [[CrossRef](#)]

38. Pei, H.; Li, F.; Wan, Y.; Wei, M.; Liu, H.; Su, Y.; Chen, N.; Huang, Q.; Fan, C. Designed Diblock Oligonucleotide for the Synthesis of Spatially Isolated and Highly Hybridizable Functionalization of DNA–Gold Nanoparticle Nanoconjugates. *J. Am. Chem. Soc.* **2012**, *134*, 11876–11879. [[CrossRef](#)]
39. Schreiner, S.M.; Shudy, D.F.; Hatch, A.L.; Opdahl, A.; Whitman, L.J.; Petrovykh, D.Y. Controlled and Efficient Hybridization Achieved with DNA Probes Immobilized Solely through Preferential DNA-Substrate Interactions. *Anal. Chem.* **2010**, *82*, 2803–2810. [[CrossRef](#)]
40. Han, W.; Liao, S.; Zhang, C.; Ding, H.; Wu, Z.; Shen, G.; Yu, R. Highly Sensitive Fluorometric Assay Method for Acetylcholine-sterase Inhibitor Based on Nile Red-Adsorbed Gold Nanoparticles. *Chin. J. Chem.* **2013**, *31*, 1072–1078. [[CrossRef](#)]
41. Yang, Y.; Mohamed Asiri, A.; Du, D.; Lin, Y. Acetylcholinesterase biosensor based on a gold nanoparticle–polypyrrole–reduced graphene oxide nanocomposite modified electrode for the amperometric detection of organophosphorus pesticides. *Analyst* **2014**, *139*, 3055–3060. [[CrossRef](#)]
42. Bai, W.; Zhu, C.; Liu, J.; Yan, M.; Yang, S.; Chen, A. Gold nanoparticle–based colorimetric aptasensor for rapid detection of six organophosphorous pesticides. *Environ. Toxicol. Chem.* **2015**, *34*, 2244–2249. [[CrossRef](#)]
43. Parambil, K.; Lisha, A.; Pradeep, T. Enhanced visual detection of pesticides using gold nanoparticles. *J. Environ. Sci. Health Part B* **2009**, *44*, 697–705.
44. Wang, Y.; Zhang, S.; Du, D.; Shao, Y.; Li, Z.; Wang, J.; Englehard, M.; Li, J.; Lin, H. Self Assembly of Ace-tylcholinesterase on a Gold Nanoparticles–Graphene Nanosheet Hybrid for Organophosphate Pesticide Detection Using Polyelectrolyte as a Linker. *J. Mater. Chem.* **2011**, *21*, 5319–5325. [[CrossRef](#)]
45. Du, D.; Chen, S.; Cai, J.; Zhang, A. Immobilization of Acetylcholinesterase on Gold Nanoparticles Embedded in Sol-Gel Film for Amperometric Detection of Organo-phosphorous. *Biosens. Bioelectron.* **2007**, *23*, 130–134. [[CrossRef](#)] [[PubMed](#)]



© 2018 by the authors. Licensee MDPI, Basel, Switzerland. This article is an open access article distributed under the terms and conditions of the Creative Commons Attribution (CC BY) license (<http://creativecommons.org/licenses/by/4.0/>).